doi:10.1017/S1431927621009405
Microsc. Microanal. 27 (Suppl 1), 2021

Atomic-scale deciphering the defect-related structure and doping behavior of transition metal in SnO_2 nanoparticles

Woo-Sung Jang, Young-Min Kim

Sungkyunkwan University, South Korea

Metal oxide nanoparticles (MO NPs) display catalytic properties similar to those of metal catalysts and have, thus, been used as efficient photocatalysts for several decades, particularly because they can be used as stable catalysts with various forms (for example, size and shape).[1-5] Nowadays, there are concerns about the continued and stable supply of energy, as well as interest in methods that enable flexible responses to energy demand; consequently, new catalyst materials are urgently required and existing catalyst materials should be improved by metal or cation doping, particularly with regard to visible-light photocatalysts.[6-10] Metal or cation doping on photocatalysts can improve the catalytic activity modulated by changing the number of oxygen vacancy, which closely related with the surface area covered with active sites that promote surface chemical reactions.[11] In line with this strategy, we synthesized SnO_2 NPs doped with Fe and Cr, which have been demonstrated to be the most feasible dopant candidates and annealed the samples at 300 °C which is well-crystallized temperature as a result of checking by XRD peak intensity and changes the size of MO NPs to be small.[12-15] Generally, as doping with transition metal on the NPs, the trivalent dopants make ionic defects which are substituted on the tetravalent cation sites of metal oxide NPs. This result suggests that the substitution of transition metal ions in the lattice can result the formation of oxygen vacancy.[16, 17] In addition, some previous works indicated that ion radii and transition metal dopants formation energy can be the important role in what kind of defects in NPs for catalytic property.[18] However, there are many different ways to implant the transition metal dopants in octahedral oxygen voids and the only way for investigating the doping behavior of transition metal was calculation until now. Therefore, direct observation at the atomic scale for transition metal dopants position and spectroscopy on the surface region for the difference in the distribution of oxygen vacancies are important analysis when deciphering doping behavior of transition metal in SnO_2 NPs.

In this study, we experimentally and computationally demonstrated the doping behavior of transition metal in SnO_2 NPs. After confirming the surface structures of three NPs (SnO_2 NPs doped with two transition metals (Fe or Fe) annealed at 300 °C) using TEM, we first assessed their catalytic capacities for the oxidation of thiophenol (TP) under 365-nm ultraviolet (UV) light illumination using high-resolution photoemission spectroscopy (HRPES). We investigated the degradation of 4-chlorophenol (4-CP), phenol and 2,4-dichlorophenol (2,4-DCP) under illumination by a 300-W arc lamp with a 320 nm cut-off filter for all synthesized NPs to estimate how dense atomic defects, which actively participated in the catalytic decomposition process, were formed on the surface of the NPs. And then, we used scanning transmission electron microscopy (STEM) which is able to compare the morphology, atomic structure and ionic defect imaging of three NPs combined with energy dispersive X-ray spectroscopy (EDX), scanning transmission X-ray microscopy (STXM) electron energy loss spectroscopy (EELS), and density functional theroy (DFT) calculations.

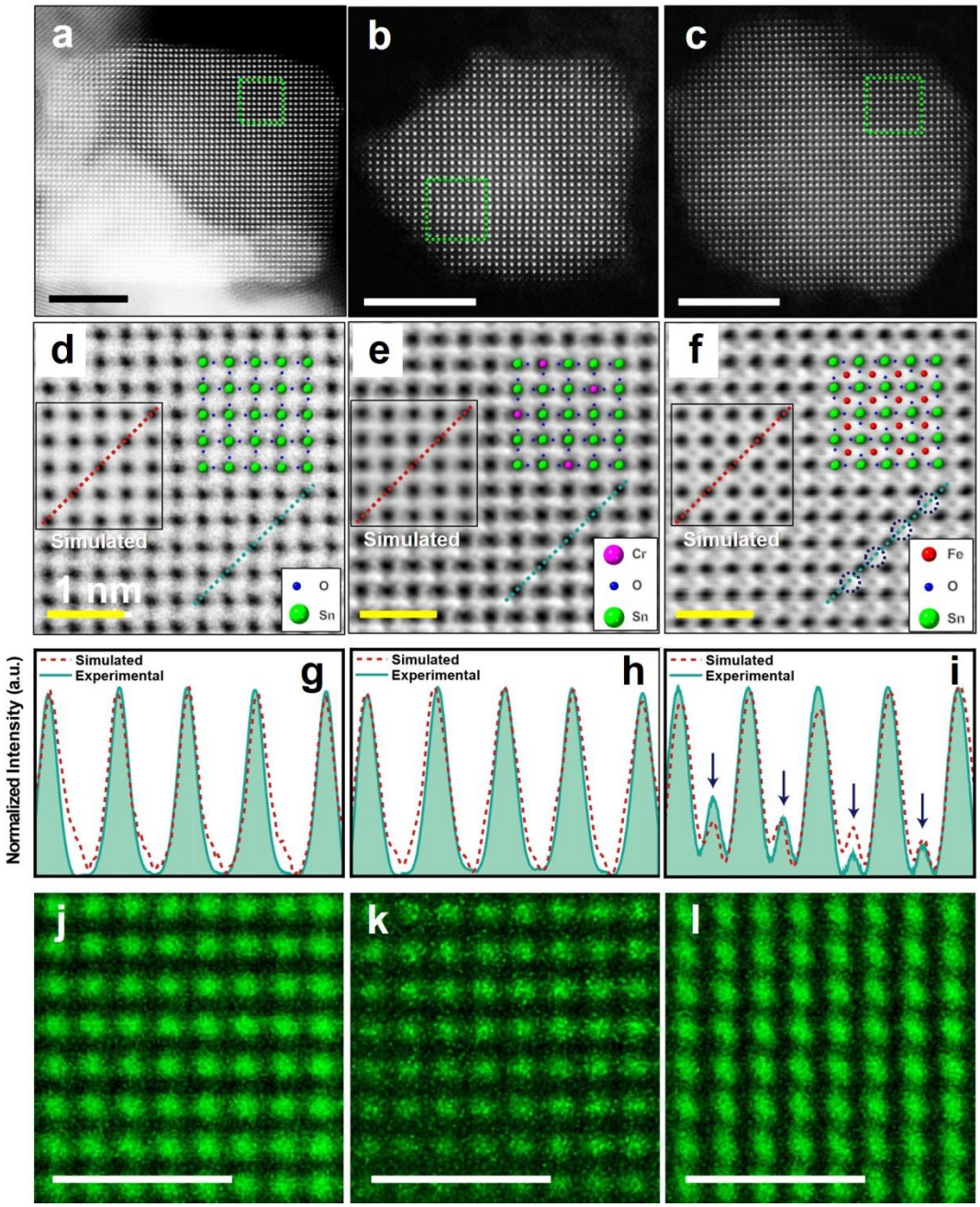

Figure 1. a-c) ADF-STEM images showing the overall morphologies of the SnO_2 NPs. Scale bar: 5 nm. a,d,g) Pristine and b,e,h) Cr- and c,f,i) Fe-doped SnO_2, respectively. d-f) Enlarged ABF-STEM images containing QSTEM simulation showing typical atomic structure of individual NPs, which shows the excellent match with the [001] rutile structure of SnO_2 (see superimposed atomic models; green for Sn, blue for O, magenta for Cr and red for Fe). Scale bar: 1 nm. These images showing doping behavior of Cr and Fe in the SnO_2 lattice structure. g-i) Comparison of three intensity profiles from different samples within the SnO_2 NP. Red dot lines and green profiles in each graph represent the simulation and experimental intensity profiles, respectively. j-l) Atomic-scale EDX mapping for Sn L edge peak. Scale bar: 5 Å.

https://doi.org/10.1017/S1431927621009405 Published online by Cambridge University Press

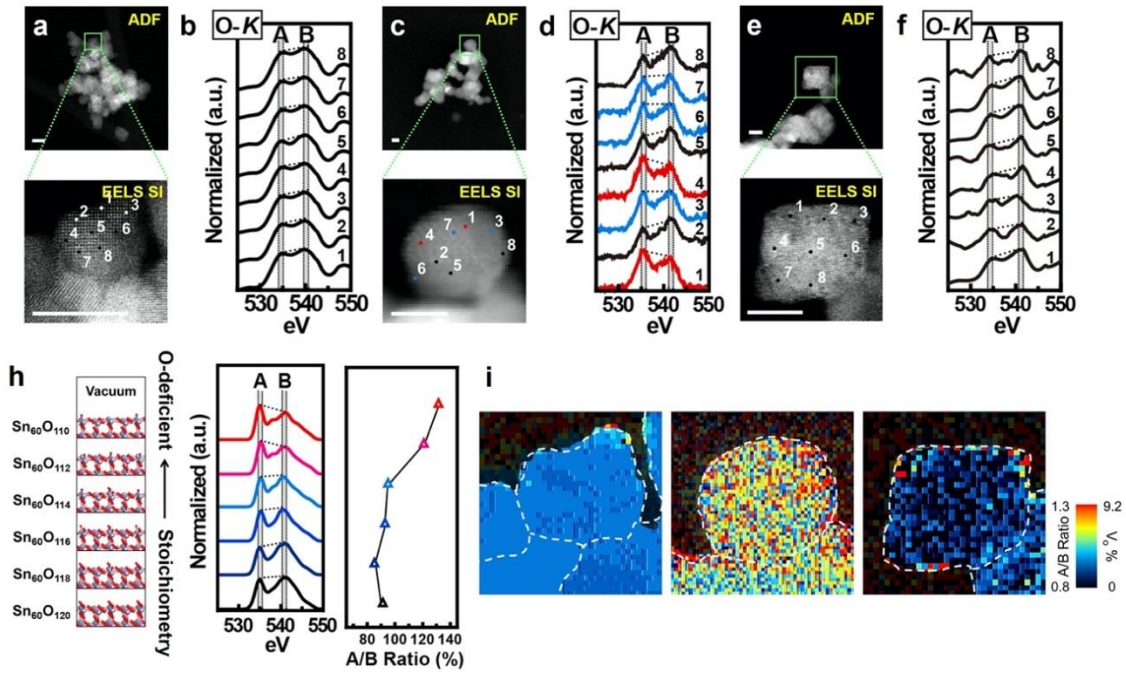

Figure 2. a, c, e) Low-magnification ADF-STEM images (upper panel) and STEM-EELS spectrum imaging (SI) data (lower panel) of the pristine SnO_2, Cr- and Fe-doped SnO_2 NPs respectively. b, d, f) O *K* ELNES spectra extracted from local positions within the respective pristine, Cr- and Fe-doped SnO_2 NPs. Note that black, blue and red spectra show a different level of oxygen content in the positions within the NPs and those are similar to O *K* ELNES profiles of SnO_2, SnO_{2-x} and SnO respectively [reference]. The dimensions of a single pixel in the EELS SI data for the pristine SnO_2, Cr- and Fe-doped SnO_2 NPs are corresponding to 0.45 × 0.45 nm^2, 0.67 × 0.67 nm^2 and 0.47 × 0.47 nm^2, respectively. h) Schematics of gradually decreasing oxygen contents in SnO_2 surface, calculated O *K*-edge X-ray absorption near edge structure (XANES) spectra of stoichiometric (black line), reduced (blue line) and oxygen deficient (red line) SnO_2 and A/B peak intensity ratio between the absorption peak A and B. i) The local oxygen contents mapping for Pristine, Cr- and Fe-doped SnO_2, respectively.

References

[1] A. V. Nikam, B. L. V. Prasad, A. A. Kulkarni, *Crystengcomm* **2018**, *20*, 5091.
[2] K. Huang, Y. Sun, Y. Zhang, X. Wang, W. Zhang, S. Feng, *Advanced Materials* **2019**, *31*, 1801430.
[3] A. A. AbdelHamid, Y. Yu, J. Yang, J. Y. Ying, *Advanced Materials* **2017**, *29*, 1701427.
[4] S. Kattel, P. Liu, J. G. Chen, *J Am Chem Soc* **2017**, *139*, 9739.
[5] D. Dissanayake, L. A. Achola, P. Kerns, D. Rathnayake, J. He, J. Macharia, S. L. Suib, *Applied Catalysis B: Environmental* **2019**, *249*, 32.
[6] A. Tricoli, M. Graf, S. E. Pratsinis, *Adv Funct Mater* **2008**, *18*, 1969.
[7] B. Tu, Y. Shao, W. Chen, Y. Wu, X. Li, Y. He, J. Li, F. Liu, Z. Zhang, Y. Lin, X. Lan, L. Xu, X. Shi, A. M. C. Ng, H. Li, L. W. Chung, A. B. Djurišić, Z. He, *Advanced Materials* **2019**, *31*, 1805944.
[8] L. Yang, J. Huang, L. Shi, L. Cao, H. Liu, Y. Liu, Y. Li, H. Song, Y. Jie, J. Ye, *Applied Catalysis B: Environmental* **2018**, *221*, 670.
[9] R. Xie, X. Meng, P. Sun, J. Niu, W. Jiang, L. Bottomley, D. Li, Y. Chen, J. Crittenden, *Applied Catalysis B: Environmental* **2017**, *203*, 515.
[10] B. Zhang, Z. Guo, Z. Zuo, W. Pan, J. Zhang, *Applied Catalysis B: Environmental* **2018**, *239*, 441.
[11] T. Cao, T. Xia, L. Zhou, G. Li, X. Chen, H. Tian, J. Zhao, J.-o. Wang, W. Zhang, S. Li, S. Meng, H. Guo, *Journal of Physics D: Applied Physics* **2020**, *53*, 424001.

https://doi.org/10.1017/S1431927621009405 Published online by Cambridge University Press

[12] J. A. Toledo-Antonio, R. Gutiérrez-Baez, P. J. Sebastian, A. Vázquez, *J Solid State Chem* **2003**, *174*, 241.
[13] C. Borras, C. Berzoy, J. Mostany, J. C. Herrera, B. R. Scharifker, *Applied Catalysis B: Environmental* **2007**, *72*, 98.
[14] H.-C. Chiu, C.-S. Yeh, *The Journal of Physical Chemistry C* **2007**, *111*, 7256.
[15] S. A. Arote, V. Tabhane, S. D. Gunjal, K. C. Mohite, H. Pathan, *Macromolecular Symposia* **2015**, *347*, 75.
[16] J. Chen, M. Yao, X. Wang, *J Nanopart Res* **2008**, *10*, 163.
[17] K. Nomura, C. A. Barrero, J. Sakuma, M. Takeda, *Physical Review B* **2007**, *75*, 184411.
[18] D. Misra, S. K. Yadav, *Sci Rep-Uk* **2019**, *9*, 12593.

https://doi.org/10.1017/S1431927621009405 Published online by Cambridge University Press